

# Phonon dispersion and lifetimes in $MgB_2$

Abhay Shukla,<sup>1</sup> Matteo Calandra,<sup>1</sup> Matteo d'Antonio,<sup>2</sup> Michele Lazzari,<sup>1</sup> Francesco Muzzi,<sup>1</sup> Christophe Bellin,<sup>1</sup> Michael Kirsch,<sup>2</sup> J. Karpinski,<sup>3</sup> S. M. Kazakov,<sup>3</sup> J. Jun,<sup>3</sup> D. Dagheno,<sup>4</sup> and K. Parlinski<sup>5</sup>

<sup>1</sup>Laboratoire de Mineralogie-Cristallographie, case 115, 4 Place Jussieu, 75252, Paris cedex 05, France

<sup>2</sup>European Synchrotron Radiation Facility, BP 220, F-38043 Grenoble cedex, France

<sup>3</sup>Solid State Physics Laboratory, ETH, CH-8093 Zurich, Switzerland

<sup>4</sup>INFM - Dipartimento di Fisica, Politecnico di Torino, C. Duca degli Abruzzi 24, 10129 Torino, Italy

<sup>5</sup>Institute of Nuclear Physics, ul. Radzikowskiego, 152, 31-342, Cracow, Poland.

(Dated: April 4, 2019)

We measure phonon dispersion and linewidth in a single crystal of  $MgB_2$  along the  $\bar{A}$  and  $\bar{M}$  directions using inelastic X-ray scattering. A nonalocal broadening of the  $E_{2g}$  phonon mode is found along  $\bar{A}$  only. We use Density Functional Theory to compute the effect of both electron-phonon coupling and anharmonicity on the linewidth, obtaining excellent agreement with experiment. The dominant contribution to the linewidth is always the electron-phonon coupling.

PACS numbers: 63.20.Dj, 63.20.Kr, 78.70.Lk, 71.15.Mb

The discovery of 39 K superconductivity in  $MgB_2$  [1] has led to in-depth study of the material and a picture has emerged of a phonon-mediated superconductor with multiple gaps [2], strong electron-phonon coupling (EPC) [3, 4, 5, 6], and anharmonicity [6, 7, 8]. However no measurements exist concerning either phonon dispersion or the evolution of phonon lifetimes over the Brillouin Zone (BZ), due to the absence of large single crystals. Neutron scattering experiments with powder samples [7, 9] have been limited to the determination of phonon density of states. Raman spectroscopy, which is restricted to the BZ center, has shown that the optical mode with  $E_{2g}$  symmetry, corresponding to in-plane distortions of the Boron hexagons, is strongly damped [10, 11, 12, 13].

Phonon damping can be attributed to two different mechanisms: (i) the decay of a phonon into electron-hole pairs mediated by EPC [14], or (ii) the phonon-phonon interaction due to anharmonicity [15]. The linewidth (the inverse of the lifetime) of a given phonon is the sum of these contributions. It has been suggested [14] that the contribution of each phonon mode to EPC over the BZ can be directly determined from the measured linewidth. This is however subject to the possibility of neglecting the damping related to anharmonicity, an approximation that has been criticized [16]. In principle this possibility is even more questionable for  $MgB_2$  where the presence of strong anharmonicity has been suggested in many calculations [6, 7, 8].

In this work we present the first measured phonon dispersion curves and linewidths along two main directions in the BZ,  $\bar{A}$  and  $\bar{M}$ . We circumvented the problem of sample size by using high resolution inelastic scattering of a focused and intense X-ray beam at the European Synchrotron Radiation Facility (beam line ID 28), a technique [17] successfully used in single crystalline samples and in particular for the measurement of high energy optical modes [18]. To better understand the physical mechanisms governing the measured phenomena we cal-

culated phonon dispersion and the contributions of EPC and anharmonicity to the linewidth using Density Functional Theory (DFT).

Though single crystals of  $MgB_2$  remain small, samples suitable for inelastic X-ray scattering experiments have recently become available. The crystal used in our experiment was grown at a pressure of 30–35 kbar. A mixture of Mg and B was put into a BN container in a cubic anvil device. The temperature was increased during one hour up to a maximum of 1700–1800 C, kept stable for 1–3 hours and decreased during 1–2 hours. As a result plate-like  $MgB_2$  crystals were formed of which we used a sample of about 400 x 470 x 40  $\mu\text{m}^3$ ; with a measured in-plane mosaicity of 0.007°. The beam incident on the sample was obtained from a high-resolution Silicon backscattering monochromator using the (8 8 8) reflection at an incident energy of 15.816 keV. The X-ray beam was focused onto the sample by a toroidal mirror into a spot of 270 x 90  $\mu\text{m}^2$  (horizontal/vertical), full width at half maximum (FWHM). Slits before the sample further limited the vertical beam size to 30  $\mu\text{m}$ . The scattered photons were analyzed in energy by five spherical silicon crystal analyzers operating at the same reflection order and mounted in pseudo Rowland circle geometry. Depending on the type of measurement all or only one of these analyzers were used. The total energy resolution was 6.1 meV FWHM, as determined by a fit to a Lorentian lineshape. The momentum transfer  $Q$  was selected by rotating the 7 m long analyzer arm around the sample position, in the horizontal plane, which also contained the linear x-ray polarization vector of the incident beam. The momentum resolution was set to 0.04  $\text{\AA}^{-1}$  in the horizontal direction and 0.07  $\text{\AA}^{-1}$  in the vertical direction. Measurements were performed in two different geometries. i) For the  $\bar{A}$  direction,  $Q = (1/2, 0, 0)$ , in a most transverse configuration, i.e. with  $Q \perp q \perp 0$ , where  $q = (0, 0, 1)$  is the phonon wavevector, ii) For the  $\bar{M}$  direction,  $Q = (1/1, 0, 0)$ , such that both transverse and longitudinal

configurations were accessible. All measurements were made at a temperature of 300K. The measured points in the BZ were chosen so as to maximize count-rate in regions with a favorable structure factor while respecting the reciprocal space attainable with the spectrometer.

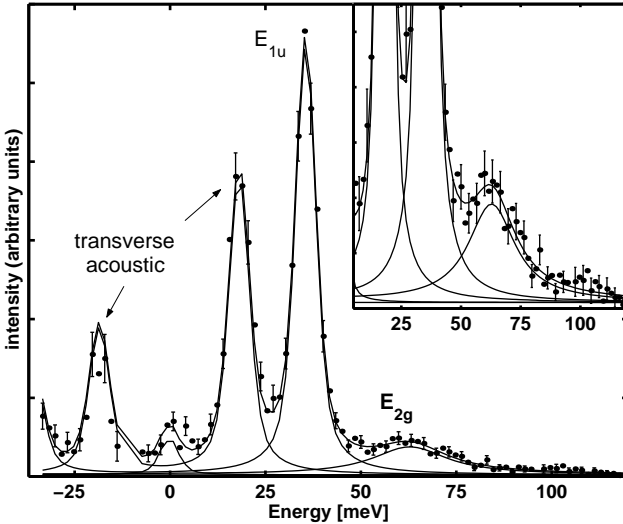


FIG. 1: Energy loss scan in almost transverse geometry measured at  $Q = (1 2 0.3)$  corresponding to  $0.6 \text{ \AA}$ . The data, normalized to the incident flux, are shown with the least-squares. Three doubly degenerate modes with in-plane polarization are detected. For the acoustic mode both Stokes and anti-Stokes peaks are visible. The broad peak corresponds to the damped  $E_{2g}$  mode and is shown in greater detail in the inset. The peak at zero is due to diffuse scattering.

In Fig. 1 we show data taken at the  $0.6 \text{ \AA}$  point in the BZ. The acoustic mode as well as the lower energy optical mode ( $E_{1u}$ ) are visible as resolution-limited peaks. Most importantly, a broad peak is observed at higher energy loss, corresponding to the  $E_{2g}$  mode. Least square fits to sums of Lorentzian functions with FWHM corresponding to the experimental resolution for the resolution-limited peaks and a free parameter for the strongly damped phonon yield the dispersion as well as the linewidth variation over the BZ. Despite statistical limitations (3-6 counts per minute on this peak along  $\text{--A}$ ) and tails of the peaks from the stronger, low energy phonons, the peak energy as well as the linewidth can be estimated with reasonable confidence.

Fig. 2 shows a similar energy loss scan at the  $0.8 \text{ \AA}$  point in the BZ. Two strong acoustic modes are seen between 25 and 50 meV. At higher energy loss the signal is weaker and composed of 4 peaks. The clearly resolved peak at 80 meV is the upper  $E_{1u}$  branch. The small shoulder at about 90 meV is the lower  $E_{2g}$  branch. The sharp drop of the shoulder clearly indicates that the  $E_{2g}$  linewidth is now much reduced and indeed the fit predicts a resolution-limited peak. Though statistics and

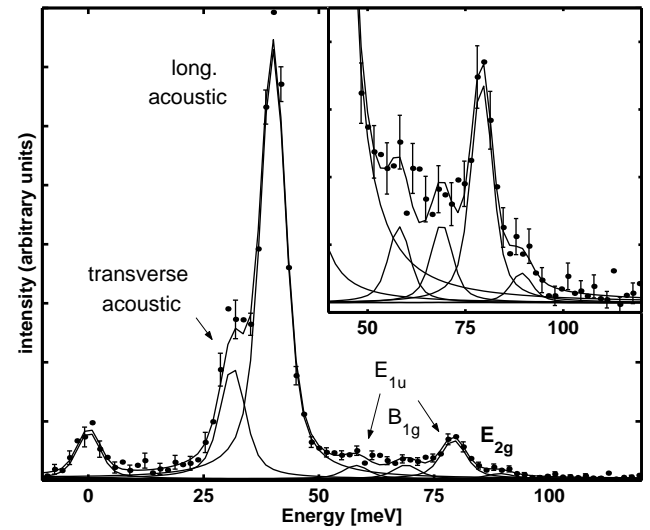


FIG. 2: Energy loss scan, measured at  $Q = (1 1 0.4)$  corresponding to  $0.8 \text{ \AA}$  with the least-squares fit. Both longitudinal and transverse modes with in-plane polarization are detected.

limited resolution do not completely preclude line broadening, this is necessarily small. Finally two more peaks are found between 50 and 75 meV, the lower energy one corresponding to the lower  $E_{1u}$  branch, while the higher one is identified as being the transverse  $B_{1g}$  mode, polarized along the c axis and visible only because of the vertical acceptance of the analyzer.

Similar analysis was done for several points along  $\text{--A}$  and  $\text{--M}$  in order to experimentally determine the phonon dispersion and the linewidths. The experimental phonon dispersion is shown in the bottom panel of Fig. 3 (circles). The large error bars in some cases are due to uncertainty introduced by ill-resolved peaks. In the region near the M point we detect the lower  $E_{2g}$  branch. In the configuration used, the acoustic modes are strong and visible over the whole BZ, while the optical modes become visible only near the zone boundary due to strengthening of the related structure factor. The linewidth of the visible  $E_{2g}$  branch, shown in the top panel of Fig. 3, is strongly anisotropic in the BZ. Along  $\text{--A}$  it is particularly large (ranging from 20 to 28 meV), while along  $\text{--M}$  it is below the experimental resolution, i.e. at least 5 times smaller than along  $\text{--A}$ . The experimental error bars are shown and correspond to a relative error of about 20%. Near the zone center this error increases due to stronger tails of the low energy phonons.

Electronic structure calculation [19] were performed using DFT in the generalized gradient approximation [20]. We used norm conserving pseudo-potentials [21]. For Mg we used non-linear core corrections [22] and we treated the 2s, 2p levels as core states. The wavefunctions were expanded in plane waves using a 35 Ry

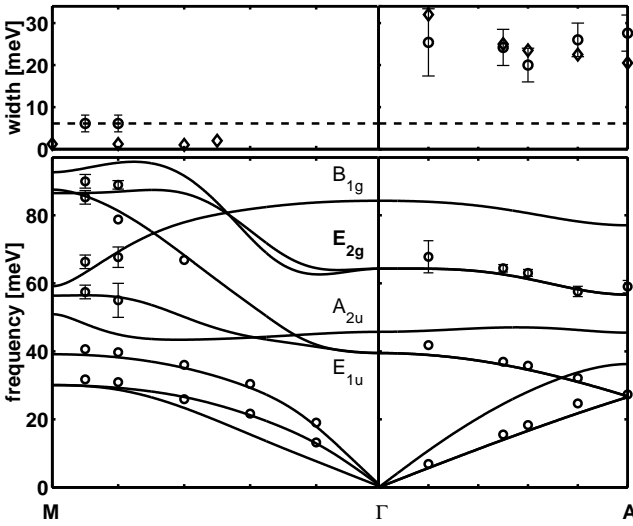


FIG. 3: Bottom : Experimental (circles) and theoretical phonon dispersion (solid line) in  $MgB_2$  along  $-A$  and  $-M$ . The optical modes are labeled according to the symmetry at the point. The highest energy acoustic branch is the longitudinal one. Top: Linewidth of the  $E_{2g}$  mode. The experimental linewidth (circles) is large along  $-A$  and below the experimental resolution (shown by the dashed line) near the  $M$  point. The theoretical result (diamonds) for the electron-phonon coupling contribution to the linewidth is also shown.

cuto . The calculations were performed with the experimental crystal structure, namely  $a = 3.083\text{ \AA}$  and  $c/a = 1.142$ . The harmonic phonon frequencies were computed in the linear response [23]. We used a  $16 \times 16 \times 16$  Monkhorst-Pack grid for the electronic BZ integration and first order Hemeite-Gaussian smearing [24] of  $0.025$  Ry. The dynamical matrix at a given point of the BZ was obtained from a Fourier interpolation of the dynamical matrices computed on a  $6 \times 6 \times 4$  phonon mesh. The resulting phonon frequencies are shown in Fig. 3 and are in good agreement with a recent calculation [10]. The agreement with experiment is remarkable.

The contribution to the FWHM linewidth  $\omega_q$  at momentum  $q$  for the phonon mode due to the electron-phonon interaction can be written as [14]:

$$\omega_q = \frac{4 \pi q}{N_k} \sum_{k, n, m} \langle \mathbf{g}_{kn, k+qm} \rangle \langle \mathbf{u}_k \rangle \langle \mathbf{u}_m \rangle \quad (1)$$

where the sum is extended over the BZ,  $N_k$  is the number of k-points in the sum, and  $\omega_{kn}$  are the energy bands measured with respect to the Fermi level at point  $k$ . The matrix element is  $\mathbf{g}_{kn, k+qm} = \hbar \mathbf{k}_n \cdot \mathbf{V} = u_q \frac{\mathbf{k}_n + \mathbf{q}_m}{2\pi}$ , where  $u_q$  is the amplitude of the displacement of the phonon of wavevector  $q$ ,  $\omega_q$  is the phonon frequency and  $V$  is the Kohn-Sham potential.

In the calculations we used  $N_k = 30^3$  inequivalent k-points and, in Eqs. (1) and (3), we substituted the

functions with Gaussians. The electron phonon coupling  $\omega_q$  is obtained from the linewidth [14] as:

$$\omega_q = \frac{\omega_q}{2 N(0) \pi^2} ; \quad (2)$$

$N(0) = 0.354$  states/ ( $MgB_2$  eV spin) being the density of states at the Fermi level.

The second contribution to the linewidth is given by the anharmonicity in the crystal potential. At lowest order for the mode of a zone center phonon the FWHM linewidth is [15, 25, 26]:

$$\omega_q = \frac{\hbar X}{8N_q} \sum_{k, u_0, u_q, u_q} \frac{\partial^3 E}{\partial u_0 \partial u_q \partial u_q} \frac{I_q^D}{\pi^2 \omega_0 \omega_q} + I_q^A \quad (3)$$

$E$  being the total energy,  $n_q$  the Bose occupation for mode at wavevector  $q$ ,  $I_q^D = (n_q + n_q + 1) (\omega_0 \omega_q \omega_q)$  describes the decay in the two phonons and, and  $I_q^A = 2(n_q + n_q) (\omega_0 \omega_q + \omega_q)$  describes the phonon absorption and the phonon emission.

We computed the anharmonic linewidth at the high-symmetry points  $\Gamma, A, M$ . For the calculation at  $A$  we consider a  $1 \times 1 \times 2$  supercell with 6 atoms, while for the  $M$  point we use a  $2 \times 2 \times 1$  cell with 12 atoms. The third order matrices were evaluated using linear response theory and the  $2n + 1$  theorem for metals [27]. The anharmonic contribution was evaluated at 0K and 300K.

At the anharmonic linewidth is largest for the  $E_{2g}$  mode and equal to 0.16 meV at  $T = 0\text{K}$  and 0.75 meV at  $T = 300\text{K}$ . Both the values are negligible if compared with the experimental Raman linewidth of roughly 40 meV [12], suggesting that the main source of broadening is the electron-phonon interaction.

The results of the calculation of the two contributions to the linewidth at  $A$  and  $M$  are shown in Table I. At the  $A$  point the linewidth of the  $E_{2g}$  mode due to electron-phonon scattering is very large while the anharmonic contribution is more than an order of magnitude smaller. For sizable values of EPC ( $\omega_q \approx 0.1$ ) the anharmonicity is always negligible, showing that a measurement of the linewidth at  $q$  for the mode is essentially equivalent to determining  $\omega_q$ . This is unexpected since earlier theoretical work [6, 7, 8] estimates anharmonicity to be important for a different but related quantity, the frequency shift.

Since the anharmonic contribution is negligible at  $\Gamma, A, M$ , and computationally demanding, we only evaluated the EPC linewidth for the other points along the two directions. In the top panel of Fig. 3 we compare the theoretical results with the experiment for the  $E_{2g}$  branch along  $-A$  and  $-M$ , obtaining good agreement with experiment. In particular along  $-M$  the theoretical linewidth is much below the experimental resolution and in fact we measured a resolution limited linewidth. The large linewidth along  $-A$  is determined by the large

M				A			
0	300	0	300	0	300	0	300
0.00	0.06	0.00	0.00	0.00	0.08	0.00	0.00
0.00	0.08	0.01	0.01	0.00	0.08	0.00	0.00
0.02	0.10	0.06	0.02	0.00	0.31	0.08	0.05
0.12	0.38	1.13	0.20	0.00	0.31	0.08	0.05
0.06	0.20	0.00	0.00	0.02	0.15	0.84	0.28
0.07	0.24	2.34	0.30	0.02	0.13	0.08	0.02
0.26	0.41	1.06	0.06	0.10	1.17	20.35	2.83
0.45	0.69	1.21	0.07	0.10	1.17	20.35	2.83
0.47	0.72	0.08	0.00	0.13	0.23	0.05	0.00

TABLE I: Calculated linewidths (meV) due to anharmonicity at 0K (0), 300K (300) and electron-phonon interaction at M and A for all modes. Phonon frequencies increase from top to bottom.  $\alpha$  is the electron-phonon coupling.  $E_{2g}$  modes in boldface.

q	0.2 $\text{--A}$	0.5 $\text{--A}$	0.6 $\text{--A}$	0.8 $\text{--A}$	1.0 $\text{--A}$					
expt:	2.5	1.1	2.6	0.6	2.3	0.5	3.6	0.7	3.6	0.8
q										
theo:	3.32		2.80		2.77		3.12		2.83	

TABLE II: Experimental and theoretical  $q$  of each of the two degenerate  $E_{2g}$  modes along  $\text{--A}$ .

nesting factor emerging from the Fermi surfaces of the boron bonding  $p_{x,y}$  bands [4], which have a cylindrical shape with axis parallel to the  $\text{--A}$  direction. Finally, we used Eq. (2) to extract  $q$  of the  $E_{2g}$  mode along  $\text{--A}$  using the measured linewidths and frequencies together with the calculated electronic density of states. In Table II the experimental values are compared with the theoretical predictions.

In conclusion, we have measured phonon dispersion and linewidths in a sub-mm sized MgB<sub>2</sub> crystal with inelastic X-ray scattering confirming the power and versatility of this technique. Both acoustic and optical modes are measured over the Brillouin zone and we find that the  $E_{2g}$  mode is anomalously broadened along the  $\text{--A}$  line but not along  $\text{--M}$ . Our Density Functional Theory calculations of the dispersion and linewidth are in excellent agreement with experiment. They show that the dominant contribution to the broadening for all modes over the whole Brillouin zone is the electron-phonon coupling, the anharmonic contribution being much smaller. Thus phonon linewidth in MgB<sub>2</sub> is a direct measure of electron-phonon coupling. With the present experimental resolution we have extracted the electron-phonon coupling of the  $E_{2g}$  mode along  $\text{--A}$ . With better experimental resolution our procedure could be extended to all modes.

This would provide a 'mapping' of electron phonon coupling over the whole Brillouin zone and the extraction of the anisotropic Eliashberg coupling function.

We acknowledge illuminating discussions with R. S. Connelli, P. Giannozzi, M. Xu, and F. Sette. The calculations were performed at the IDRIS supercomputing center. M.C. was supported by a Marie Curie Fellowship of the European Commission, contract No. IHP-HPMF-CT-2001-01185.

---

- [1] J. Nagaoka et al, Nature (London) 410, 63 (2001).
- [2] H. J. Choi et al, Nature (London) 418, 758 (2002).
- [3] J. M. An and W. E. Pickett, Phys. Rev. Lett. 86, 4366 (2001).
- [4] J. Kortus et al, Phys. Rev. Lett., 86, 4656 (2001).
- [5] Y. Kong et al Phys. Rev. B, 64, 020501(R) (2001).
- [6] A. Y. Liu, I.I. Mazin and J. Kortus, Phys. Rev. Lett. 87, 087005 (2001).
- [7] T. Yildirim et al Phys. Rev. Lett. 87, 37001 (2001).
- [8] H. J. Choi et al, Phys. Rev. B 66, 020513 (2002)
- [9] R. Osborn et al Phys. Rev. Lett. 87, 17005 (2001)
- [10] K. P. Bohnen, R. Heid and B. Renker, Phys. Rev. Lett. 86 5771 (2001).
- [11] A. F. Goncharov et al Phys. Rev. B 64, 100509 (2001)
- [12] P. Postorino et al Phys. Rev. B 65 020507(R) (2001)
- [13] J. Hlinka et al Phys. Rev. B 64, 140503(R) (2001)
- [14] P. B. Allen, Phys. Rev. B 6, 2577 (1972), P. B. Allen and R. Silbergliitt, Phys. Rev. B 9, 4733 (1974).
- [15] J. M. Menendez and M. Cardona, Phys. Rev. B 51 (1984)
- [16] G. Grimvall, The electron-phonon interaction in metals, (North Holland, Amsterdam, 1981) p. 201.
- [17] T. Ruf et al Phys. Rev. Lett. 86, 906 (2001)
- [18] M. D'Amato et al Phys. Rev. Lett. 88, 167002 (2002).
- [19] S. Baroni, A. Dal Corso, S. de Gironcoli and P. Giannozzi, <http://www.pwscf.org>
- [20] J. P. Perdew, K. Burke, M. Ernzerhof, Phys. Rev. Lett. 77, 3865 (1996)
- [21] N. Troullier and J. L. Martins, Phys. Rev. B 43, 1993 (1991).
- [22] S. G. Louie, S. Froyen, and M. L. Cohen, Phys. Rev. B 26, 1738 (1982)
- [23] P. Giannozzi et al, Phys. Rev. B 43, 7231 (1991)
- [24] S. de Gironcoli, Phys. Rev. B 51, 6773 (1995)
- [25] A. D'Ebenedicti, S. Baroni and E. M. Olinari Phys. Rev. Lett. 75, 1819 (1995)
- [26] G. Lang et al Phys. Rev. B 59, 6182 (1999)
- [27] M. Lazzeri and S. de Gironcoli Phys. Rev. B 65, 245402 (2002). For the electronic BZ integration we used a 14 14 8, 14 14 4, 7 7 8 mesh for the calculation at  $\text{--A}$ ,  $\text{--M}$ , respectively. The third order derivative of the total energy were computed with a 4 4 2, 4 4 1 and 2 2 2 mesh of  $q$  points for  $\text{--A}$ ,  $\text{--M}$  respectively and Fourier interpolated at the points  $q$  required for the BZ summation in Eq. (3). We performed the  $q$  BZ summation using a  $20^3$  grid of inequivalent points.